International Journal of Pharmaceutics 690 (2026) 126581

Contents lists available at ScienceDirect

International Journal of Pharmaceutics

journal homepage: www.elsevier.com/locate/ijpharm

Comparison and validation of a high-throughput lipid nanoparticle production and characterization workflow

Simone Misto [a], Teresa Ferrillo [a], Sandor Balog [b], Fabiana Quaglia [a], Thomas Lee Moore [a,*]

[a] Department of Pharmacy, Università degli Studi di Napoli Federico II, Via Domenico Montesano, 49, 80131 Naples, Italy
[b] Adolphe Merkle Institute, Université de Fribourg, Chemin des Verdiers 4, 1700 Fribourg, Switzerland

ARTICLE INFO

Keywords:
Nanomedicine
Lipid nanoparticles
Automation
High-throughput
Microfluidics

ABSTRACT

Lipid nanoparticle-borne, RNA-based therapeutics have emerged as transformative tools in nanomedicine. However, to optimize lipid nanoparticle (LNP) formulations against different pathologies, it will be necessary to change LNP payload, lipid composition, and production parameters. High-throughput formulation screening provides a way to rapidly develop and assess new LNP formulations, however this requires the capacity for high-throughput LNP physico-chemical characterization methods. When considering a shift towards automated/semi-automated high-throughput methods, it is pertinent to evaluate whether such characterization is comparable to so-called "tried and true" methods, especially in the context of scaling hit formulations from the screening phase to production. Here, we show that combining a semi-automated microfluidic system with a high-throughput characterization instrument enables the rapid production and characterization of LNP. Compared to conventional methods, the high-throughput plate reader DLS provided comparable hydrodynamic diameter data and faster analysis, albeit with lower sensitivity for RNA quantification. Additionally, we conducted an independent analysis of raw autocorrelation function data from dynamic light scattering measurements to mitigate functional differences between the high-throughput and single sample instruments. Fluorescence-based assays, also capable for high-throughput workflows, were demonstrated to be more sensitive for RNA quantification. These results illustrate that high-throughput systems can streamline LNP development, and be integrated into a translational workflow, i.e. screening to identify hit formulations, transition of hit formulations to scalable production methods, and validation of screening characterization results. This integrated workflow represents an important step for RNA therapeutic development pipelines, where increasing characterization capacity can accelerate nanomedicine development.

1. Introduction

Increasingly, automation is accelerating our capacity for scientific discovery. One field that stands to benefit from innovations in laboratory automation is nanomedicine (Hickman et al., 2023; Liu et al., 2021). In fact, automation has already been applied towards high-throughput screening of nano-formulations (Fan et al., 2021) and the identification of "hit" nanomedicine formulations to advance through the development pipeline (Cui et al., 2022). However, there exists a necessity to translate currently accepted methodologies, especially in the context of nanoparticle characterization, into high-throughput and automated workflows. Moreover, in the perspective of formulation scale-up and translation, the congruence of formulations produced and characterized via high-throughput screening must be validated with downstream methodologies where screening workflows is not necessary.

Automation has existed for quite some time in the fields of chemical synthesis and development (Coley et al., 2019). However, commercially available solutions for "nano"-centric applications have only recently become available to the average scientific consumer (Cui et al., 2022; Dauer et al., 2021; Le Ru et al., 2025; Mohr et al., 2013). This includes tools that facilitate automated nanoparticle production (i.e. either through microfluidics, automated liquid handling, or other automated mixing processes), and critically, in nanoparticle characterization (Cui et al., 2022b; Shepherd et al., 2023; Yoo et al., 2025). In fact, since nanoparticles do not behave as small molecules, their physical size and colloidal behavior necessitate certain considerations, and the translation of automated workflows in nano-characterization has generally lagged behind automation in other fields of research. Here we set out to

* Corresponding author.
E-mail address: thomaslee.moore@unina.it (T.L. Moore).

https://doi.org/10.1016/j.ijpharm.2026.126581
Received 17 October 2025; Received in revised form 30 December 2025; Accepted 6 January 2026
Available online 7 January 2026

systematically compare conventional methods in nanomedicine formulation development, specifically in the context of lipid nanoparticles for the delivery of nucleic acid payloads, with high-throughput and automated solutions. In particular, we looked at a plate reader dynamic light scattering (DLS) system that combined multi-angle DLS with UV/Vis spectroscopy to evaluate nanoparticle hydrodynamic diameter, dispersity (polydispersity index, PdI), and encapsulation of RNA payloads (e.g. mRNA or siRNA). This high-throughput approach was compared to conventional techniques such as one-at-a-time DLS instrument (for hydrodynamic diameter and PdI) and the RiboGreen assay for RNA loading. Such evaluation is critical in bridging the screening phase to downstream formulation scale-up, by verifying nanoparticle quality attributes remain consistent throughout the development process.

2. Materials and methods

2.1. Materials

9-Heptadecanyl 8-((2-hydroxyethyl)[6-oxo-6-(undecyloxy)hexyl] amino) octanoate (SM-102) and dilinoleyl-methyl-4-dimethylaminobutyrate (DLin-MC3-DMA) were purchased from BLD Pharm (Hamburg, Germany). Cholesterol, ethanol, and phosphate buffered saline (PBS) were supplied from Sigma-Aldrich (Saint Louis, Missouri, USA). 1,2-Distearoyl-*sn*-glycero-3-phosphocholine (DSPC) and 1,2-Dimyristoyl-*rac*-glycero-3-methoxy polyethylene glycol-2000 (DMG-PEG_{2k}) were obtained from Avanti® Polar Lipids (Alabaster, Alabama, USA). CleanCap® EGFP mRNA was purchased from TriLink BioTechnologies (San Diego, California, USA). The Nanosphere™ size standards and Silencer™ Select Negative Control No. 1 siRNA used in this study were obtained from Thermo Fisher Scientific (Waltham, Massachusetts, USA). All reagents were used without further purification.

2.2. Nanoparticle production

Lipid nanoparticles (LNP) were prepared using the Sunshine™ microfluidic platform (Unchained Labs, Pleasanton, United States). D-Lin-MC3-DMA (or SM-102), cholesterol, DSPC and DMG-PEG_{2k} were dissolved in ethanol (EtOH) at molar percentages of 50 %, 38.5 %, 10 %, and 1.5 %, respectively, at a final total lipid concentration of 5.5 mM. The aqueous phase consisted of EGFP mRNA diluted to 17 μg/mL (or 29 μg/mL) in acetate buffer (15 mM, pH 4.0). For siRNA LNP, the aqueous phase contained scrambled siRNA at 2 μM.

The solutions were injected at a flow rate ratio of 3:1 aqueous to organic phases, at varying total flow rates (1, 2, and 3 mL/min). Solvents were mixed in a Particle Works Junction Chip (190 μm etch depth, Royston, United Kingdom) where the fluidic path was arranged in a T junction configuration. Microfluidic channels had a height of 190 μm and width of 195 μm at the fluid intersection, and after the mixing chamber the channel width expands to a width of 390 μm while maintaining a channel height of 190 μm. The resultant LNP were collected with an automated fraction collector and dialyzed at 4 °C in 1 × phosphate buffered saline (PBS, pH 7.4) to remove trace amounts of EtOH and exchange from an acidic to neutral pH.

2.3. Nanoparticle characterization

2.3.1. Nanoparticle hydrodynamic diameter, dispersity, and concentration

Nanoparticle hydrodynamic diameter (d_H) and dispersity were evaluated via dynamic light scattering (DLS) by comparing two methods: (1) A conventional single-sample DLS (singleDLS) approach using a Malvern Zetasizer Ultra and (2) a high-throughput screening DLS (htsDLS) approach using an Unchained Labs Stunner plate reader DLS. Optimal DLS settings were automatically set by the instruments, and unless otherwise stated, scattering angles were set at 173° or 143° for the singleDLS and htsDLS, respectively. To compare the d_H distribution curves of the nanoparticles between instruments, scattering intensity density plots were normalized, i.e. the intensity values were normalized between 0 and 1 according to the Eq. (1):

$$I_{norm} = \frac{I\text{-}I_{min}}{I_{max}\text{-}I_{min}} \quad (1)$$

where I is the intensity at a certain d_H (nm), I_{min} is the minimum intensity across the entire d_H distribution, and I_{max} maximum intensity value across the d_H distribution. This normalization facilitates the comparison of relative intensity distributions of the nanoparticles across instruments.

Nanoparticle concentrations were also evaluated on both the singleDLS and htsDLS, as well as via nanoparticle tracking analysis (NTA) on a Malvern NanoSight NS 300. For NTA, nanoparticle dispersity is represented by the span (Eq. (2)), rather than via PdI:

$$Span = \frac{D90\text{-}D10}{D50} \quad (2)$$

where *D90* is the size comprising up to 90 % of the volume of material of the nanoparticle size distribution, while *D50* is the size comprising up to 50 % (the median size) and *D10* is the size comprising up to 10 %. The span represents the sample's polydispersity. A low span indicates a greater particle homogeneity, while a high value reflects an increased dimensional variability.

Nominal nanoparticle concentration for standard polystyrene Nanosphere™ particles were estimated based on material properties reported by the manufacturer and simple conversion of size/mass concentration to nanoparticle concentration. Briefly, it was assumed that as-supplied standard polystyrene nanoparticles had a density of 1.05 g/cm^3 with a reported concentration of 1 w/v%. The mass of a single particle was approximated using the equation for a sphere multiplied by the density of polystyrene, with an assumed radius calculated as the nominal size divided by two. The mass concentration was then divided by the mass per nanoparticle to get an estimated nominal concentration in number of nanoparticles per volume.

2.3.2. Quantification of RNA loading

Payload concentrations were likewise evaluated via a conventional approach (the RiboGreen assay) and an automated approach (Stunner). LNP, either in Tris-EDTA buffer to quantify external (unencapsulated) RNA or in 0.5 v/v% Triton X-100 in Tris-EDTA to lyse LNP for total RNA quantification, were incubated with the Quant-IT RiboGreen reagent according to manufacturer specification. Quantitative analysis was performed by spectrofluorimetry at $\lambda_{ex}/\lambda_{em}$ 475 nm/520 nm on a ProMega GloMax Plate reader. Results are reported as actual loading (μg/mL of encapsulated mRNA or nM of encapsulated siRNA), encapsulation efficiency (internal RNA over total measured RNA) and RNA entrapment yield (% of total RNA over theoretical RNA loaded). All results are expressed as the mean value ± SD of three independent experimental replicates.

For automated total mRNA or siRNA loading, the Stunner (htsDLS) was used, which combines static light scattering (SLS), dynamic light scattering (DLS), and UV–Vis spectrophotometry in a single device. First, a library of the payloads and materials used was constructed – mRNA and siRNA were scanned at different wavelengths and over a series of dilutions. These are used by the instrument to construct a “fingerprint” of the various materials.

Practically, 2 μl of LNP sample are loaded into the specialized Stunner plate, and DLS and UV/Vis measurements are performed contemporaneously. The instrument then calculates RNA loading by spectral unmixing of the UV/Vis absorption profiles for the LNP and mRNA. Because the RiboGreen assay and Stunner rely on two mechanistically different methods to quantify RNA loading, namely UV/Vis absorption versus a fluorescent assay, a third method for quantifying RNA loading was employed, the NanoDrop, which allows rapid

measurement of UV/Vis spectra in small volumes (i.e. 1 μL). A series of RNA dilutions were measured on the NanoDrop, and the absorbance at 260 nm was recorded for RNA concentration.

The limit of detection (LOD) and limit of quantification (LOQ) for all methods of RNA measurement were calculated by Eqs. (3) and (4), respectively:

$$LOD = \frac{3.3\sigma}{m} \tag{3}$$

$$LOQ = \frac{10\sigma}{m} \tag{4}$$

where σ is the standard deviation of the blank (or lowest concentration measurement) and m is the slope of the aggregate best fit linear model (i.e. best fit curve through all standard curves combined). Standard curves for mRNA or siRNA were performed on $n \geq 5$ independent standard curves.

RNA loading was quantified via three metrics: (1) the total RNA measured, (2) the % RNA entrapment yield (% $Yield_{RNA}$), and (3) as the % encapsulation efficiency (% EE). The latter two can only be calculated via the Ribo Green assay. Total RNA is the total amount of RNA reported by the measurement method. The % RNA entrapment yield assesses the encapsulated RNA cargo (i.e. within the LNP) relative to the initial nominal total RNA concentration (i.e. the total input RNA used to prepare the formulation). Thus, the initial nominal total RNA concentration assumes no loss during the production process and represents the theoretical total concentration of RNA. The % entrapment RNA yield is estimated with Eq. (5):

$$\%Yield_{RNA} = \frac{[RNA_{tot}]\text{-}[RNA_{ext}]}{[RNA_{initial}]} \times 100 \tag{5}$$

where $[RNA_{ext}]$ is the external, unencapsulated concentration of RNA, $[RNA_{tot}]$ is the total RNA concentration measured, and $[RNA_{initial}]$ is the theoretical maximum concentration of RNA (i.e. initial amount of RNA in the formulation).

The % encapsulation efficiency (%EE) quantifies the fraction of RNA that is successfully entrapped within the nanoparticles by comparing the measured external RNA (i.e. unencapsulated RNA) that is determined by the RiboGreen assay before lysing the LNP with Triton X-100, versus the total RNA measured in the LNP after lysing with Triton X-100 (Eq. (6)).

$$\%EE = \left(1\text{-}\frac{[RNA_{ext}]}{[RNA_{tot}]}\right) \times 100 \tag{6}$$

2.4. Computation and statistics

Statistics were calculated with R version 4.4.3 “Trophy Case”. Comparison of means was performed either via a one-tailed Student’s T test or analysis of variance with post hoc Tukey’s Honestly Significant Difference (HSD) test. A significant difference was defined as a p-value < 0.05. Raw autocorrelation data was analyzed with a custom script written in Mathematica version 14.

3. Results and discussion

3.1. High-throughput workflow for nanoparticle characterization

LNP have risen to prominence thanks to their critical role in fighting the SARS-CoV-2 (COVID-19) pandemic (Cullis and Felgner, 2024, p. 60; Dolgin, 2021). This success has generated an influx of interest in developing LNP platforms for the delivery of nucleic acid payloads (e.g. siRNA, mRNA). However, the rapid optimization of an LNP formulation to deploy some nucleic acid payload against a specific pathology may depend on the systematic evaluation of many different formulation parameters.

It is critical that the quality attributes of LNP developed during an automated high-throughput screening process (e.g. d_H, dispersity, RNA payload loading efficiency) are as similar as possible to those results obtained when scaling the LNP development. Thus, the output of high-throughput characterization methods should match as closely as possible with those results evaluated downstream in the development process. Fig. 1 shows a conceptual schematic where single measure instruments are employed to characterize nanomedicine quality attributes, and how the all-in-one, high-throughput system can merge these analyses.

3.2. Evaluating colloidal properties of nanoparticles

3.2.1. Validating methods on standard nanoparticles

We first investigated the reliability of the htsDLS for analyzing nanoparticle colloidal properties using standard polystyrene Nanosphere™ with nominal sizes of 60 and 200 nm. Fig. 2 shows the d_H and dispersity results of multi-angle DLS performed on 60 nm or 200 nm polystyrene standard nanoparticles. It was observed that d_H and polydispersity index (PdI) values for both instruments tended to converge as the scattering angle increased, likely because measuring at backscattering angles minimizes the effect of large contaminants and multiple scattering events (Stetefeld et al., 2016). Comparisons of nanoparticle d_H measurements were thereafter made with the backscatter angle. To simplify comparison between instruments, the intensity values of the backscatter d_H distributions were normalized (Eq. (1)). Size distributions on the singleDLS showed a much broader peak width compared to those measured on the htsDLS (Fig. 2A, right and **2B**, right), which is due to differences in instrument scattering angle (143° or 173° for htsDLS or singleDLS, respectively), laser wavelength (660 nm vs 633 nm for the htsDLS and singleDLS, respectively), and the particular algorithm/workflow that the two instruments utilize for extracting d_H distributions from the raw autocorrelation function data.

In fact, it is important to point out the fundamental differences between the singleDLS and htsDLS. As stated above, both instruments employ different backscatter angles and laser wavelengths. However, more practically, the singleDLS measures concentration of a large volume (e.g. ~ 1 mL depending on the type of cuvette used), while the htsDLS uses a minimal volume of 2 μL. The htsDLS here also requires a specialized well plate where the solution is loaded into a capillary with two windows, one used for multi-angle DLS measurements and the other for UV/Vis measurements. This is in contrast with other high-throughput DLS methods that utilize conventional well-plates (Dauer et al., 2021).

To this last point, we implemented an instrument-independent approach to evaluate the raw autocorrelation data to calculate particle d_H and dispersity. The rationale was to remove any bias associated with the instrument data processing and evaluate the particle d_H and dispersity based purely on the signal (autocorrelation function) data. Here, the method of cumulants approach was applied which is a classical approach in DLS used to extract particle d_H information (Koppel, 1972; Stetefeld et al., 2016). Traditionally, this involves fitting the logarithm of the field correlation function to a polynomial, yielding cumulants like mean and variance. However, this linear method is sensitive to noise, requires data truncation, and assumes a fixed baseline. Frisken (2001) and Mailer et al. (2015) proposed a nonlinear reformulation using moments about the mean, which allows for more robust and accurate fitting (especially with modern computational tools). This nonlinear approach fits the entire dataset, treats the baseline as a free parameter, and performs well even with noisy data. It reliably estimates the mean and variance of the decay rate distribution for moderate polydisperse samples (up to approx. PdI of 0.3). Therefore, the method is best suited for monomodal, narrow distributions and is limited in resolving multimodal or broad distributions. Overall, nonlinear cumulant analysis offers a practical balance between simplicity and accuracy in particle sizing. This approach was applied to raw data from both the htsDLS and singleDLS, thus enabling the comparison of reported d_H and PdI across both instruments and analysis methods.

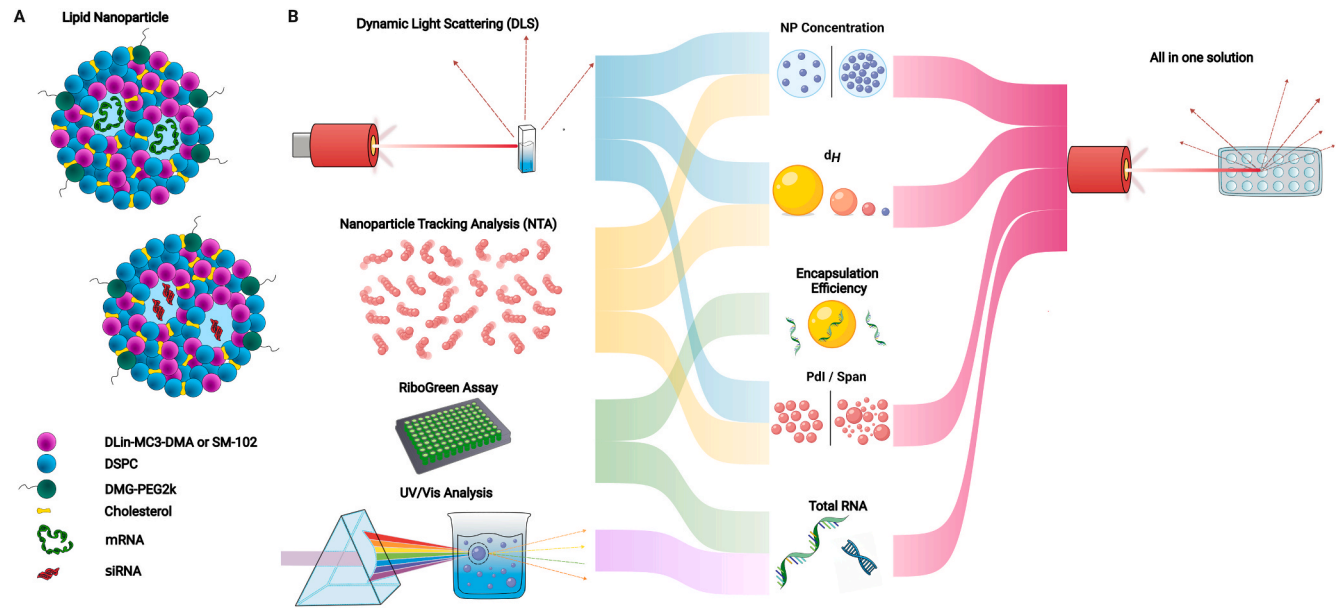

Fig. 1. Workflow for the preparation and characterization of LNP. (A) The figure shows the self-assembly of an LNP using four lipids (DLin-MC3-DMA, DSPC, DMG-PEG_{2k}, cholesterol) and a nucleic acid payload (mRNA or siRNA). (B) The characterization of the LNP was carried out by comparing two approaches: an "All in one solution" (htsDLS) approach that integrates the essential analyses, and another in which the individual dedicated platforms were used for each specific analysis. The latter include Dynamic Light Scattering (DLS) for d_H and PdI, Nanoparticle Tracking Analysis (NTA) for particle concentration, and RiboGreen Assay and UV/Vis analysis for cargo encapsulation efficiency.

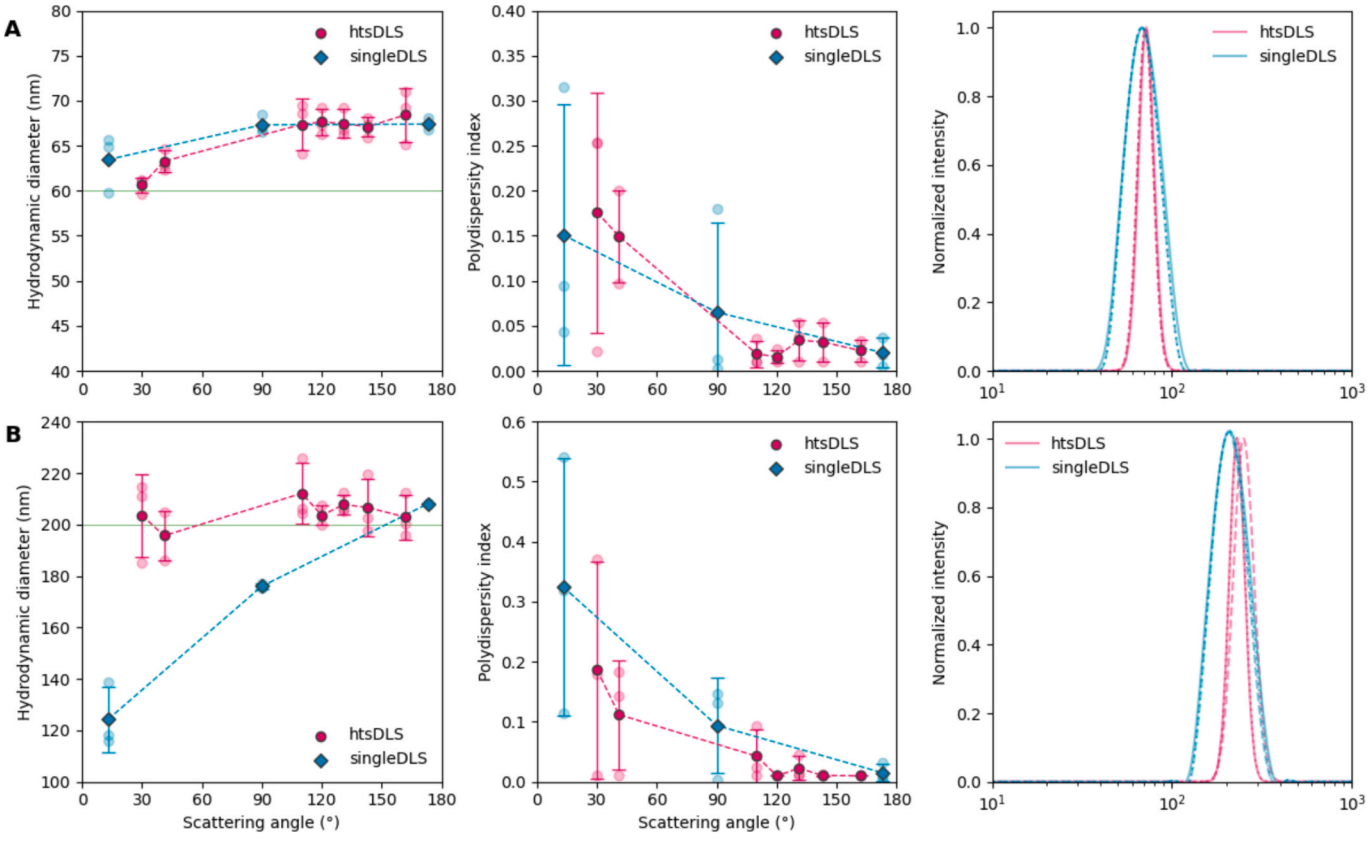

Fig. 2. Dynamic light scattering analysis of NIST-standard polystyrene Nanosphere™ on either the singleDLS or htsDLS plate reader DLS with nominal sizes of (A) 60 nm and (B) 200 nm. d_H (left column) and polydispersity index (PdI, center column) were measured over multiple scattering angles. d_H and PdI values for both particle sizes and instruments converged at the backscatter angle (i.e. 143° and 173° for htsDLS and singleDLS, respectively), the backscatter angle was used to compare d_H distributions across instruments (right column). For back scatter measurements (right column), solid, dashed, and dotted lines represent three independent experimental replicates. Horizontal green lines represent the nominal size for either 60 nm or 200 nm Nanospheres™.

Fig. 3 shows the d_H and PdI values for either the 60 nm or 200 nm polystyrene standard particles, as reported by the instrument data processing (default) or as derived from our independent analysis of the autocorrelation data (independent). Differences in mean Z-average d_H were evaluated with analysis of variance and post-hoc Tukey's HSD. For 60 nm Nanospheres™, there was no significant difference in d_H between default and independent analysis for either the singleDLS (p-value = 0.91), or the htsDLS (p-value = 0.58). Similarly, no differences were observed in DLS measurements for Z-average d_H between singleDLS and htsDLS using the default analysis (p-value = 0.22) or the independent analysis (p-value = 0.48). For the 200 nm Nanospheres, there was no significant difference between default or independent analysis for either the singleDLS (p-value = 0.88), while for the htsDLS the differences were at the limit of signifance (p-value = 0.05). There was no significant difference found between singleDLS or htsDLS for either the default method of analysis (p-value = 0.06) or the independent analysis (p-value = 0.93). These data underscore that for both instruments the sizing results on standard samples remain consistent, even when evaluated with an independent computation of d_H distribution. A similar analysis revealed that there were no significant differences in any of the PdI values reported.

3.2.2. *Measuring standard nanoparticle concentrations*

Next, a comparison between the singleDLS and htsDLS was performed to evaluate the capacity for measuring nanoparticle concentration with the Nanosphere™ standards (Austin et al., 2020). With DLS, measuring nanoparticle concentration is dependent on the relationship between particle size and scattering intensity (Vysotskii et al., 2009). Liu et al. (2008) reported the direct correlation between gold nanoparticle (spheres and rods) concentration and scattering intensity as measured by DLS. Multi-angle dynamic light scattering further enables the calculation of nanoparticle concentration based on the intensity-weighted size distribution and the scattered count rate (Austin et al., 2020). In essence, scattered count rate is derived from the mean count rate, and is dependent on particle size, concentration, scattering angle, and the differential scattering cross section. A deeper discussion on the calculation of particle concentration via DLS can be found in several reviews (Maguire et al., 2018; Shang and Gao, 2014).

The standard Nanosphere™ nanoparticles provide a means for administering nanoparticles at controlled concentrations based on the nominal size and known material properties. For comparison, nanoparticle tracking analysis (NTA) was also employed as a mechanistically different method for evaluating nanoparticle d_H (Table 1) and concentration (Fig. 4). Notably, the range of concentrations that could be measured was different for these two particles with nominal sizes of either 60 nm or 200 nm. This difference is due to the physical and optical properties of the particles and the type of detection of each instrument. Larger particles, such as the 200 nm Nanospheres™, scatter light more strongly and are thus more easily detected by optical scattering techniques such as the singleDLS and htsDLS. Conversely, smaller particles like the 60 nm nanospheres generate weaker signals that are more prone to background noise, limiting the capability of the instruments to accurately detect and quantify them. For the 200 nm Nanosphere™, the htsDLS was almost perfectly correlated between the nominal size and measured concentrations. Likewise, the singleDLS was in good agreement with the nominal particle concentration until the highest concentration of 10E11 NP/mL. This is likely because the larger particles have stronger optical scattering, thus enabling the htsDLS to detect concentrations close to nominal values. For 60 nm Nanospheres, both the singleDLS and htsDLS reported concentrations below the nominal concentration, with the htsDLS under-reporting the concentration more than the singleDLS. This underestimation by the singleDLS and htsDLS could be justified based on the principles of DLS, which evaluates concentration indirectly from the signal count rate and d_H. Moreover, DLS-based instruments systematically tend to underestimate the concentration of smaller particles compared to direct counting methods such as NTA, based on individual particle tracking, that tends to overestimate the nominal concentration, likely due to counting aggregates or smaller particles as multiple entities. These results are in line with previous reported work (Austin et al., 2020).

In Tian et al. (2024), a working particle concentration range of 10^6 – 10^9 particles/mL was recommended for measuring size/concentration with 100 nm polystyrene or SiO_2 nanoparticles. However, DLS measurements for concentrations outside of the ranges reported here, 1.0E11–1.0E13 particles/mL for 60 nm or 1.0E9–1.0E11 particles/mL for 200 nm Nanospheres™, were either too dilute or too concentrated to obtain reliable measurements. Within these concentration ranges, only one of the measurements fell outside of the recommended 10–100 NP/

Table 1
Summary of standard Nanosphere™ polystyrene nanoparticle size measurements (n = 3).

Particle	Instrument	Z-average d_H (nm)	PdI/Span
60 nm Nanosphere™	singleDLS	67 ± 1	0.020 ± 0.016
	htsDLS	67 ± 1	0.032 ± 0.022
	NTA	75 ± 5	0.153 ± 0.015[†]
200 nm Nanosphere™	singleDLS	208 ± 0.2	0.015 ± 0.014
	htsDLS	207 ± 11	0.011 ± 0.001
	NTA	187 ± 13	0.457 ± 0.100[†]

[†] Size dispersity for the NTA is reported as the "span" (Eq. (2)), not PdI.

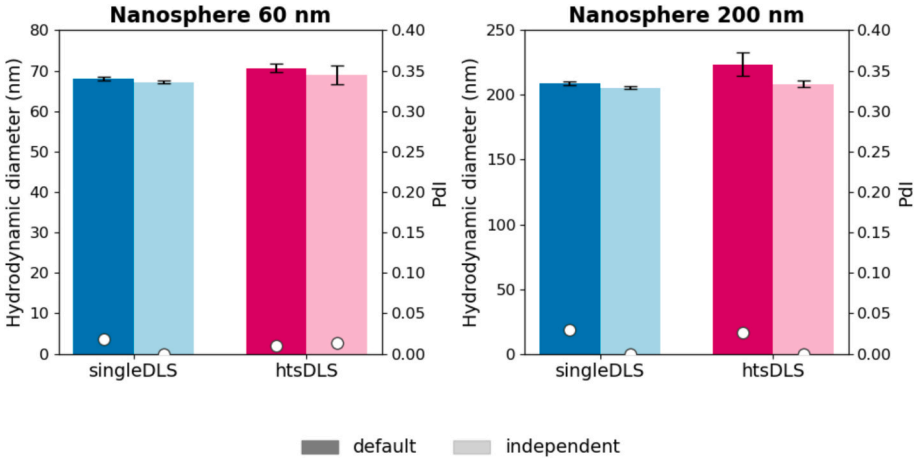

Fig. 3. Comparison between default values for d_H and polydispersity index (PdI) reported by the instruments, and those calculated independently from the raw autocorrelation function data, using nanospheres of 60 and 200 nm. Measured at backscatter angles of 173° and 143° for the singleDLS and htsDLS, respectively (n = 3).

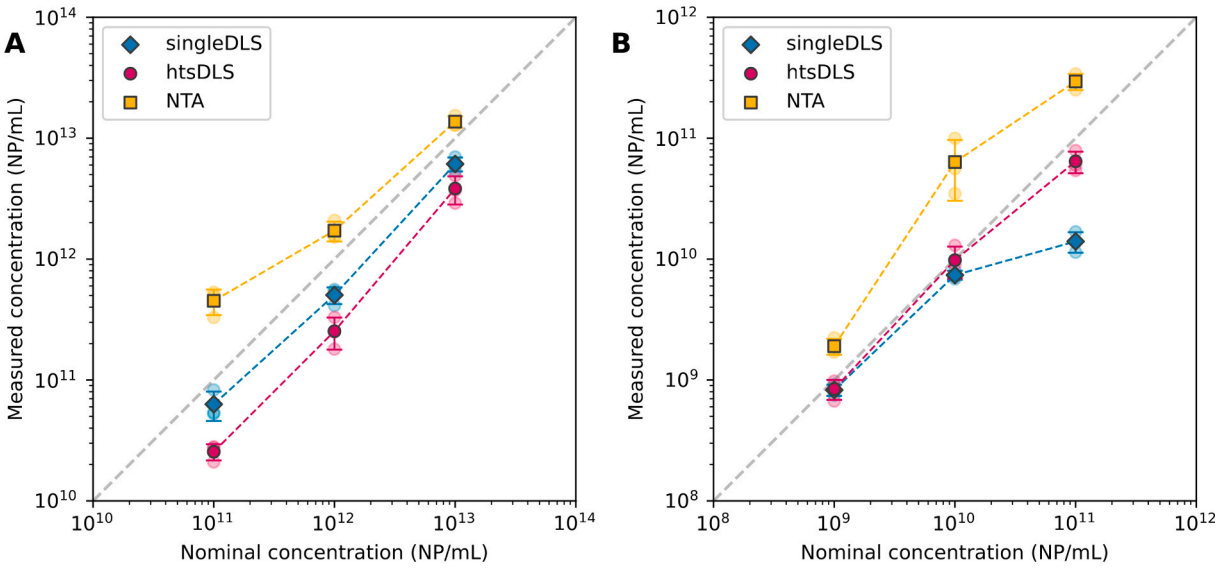

Fig. 4. Comparison of nanoparticle concentrations measured via either the singleDLS, htsDLS, or via nanoparticle tracking analysis (NTA) for (A) 60 nm or (B) 200 nm Nanosphere™ standard polystyrene nanoparticles. Solid points represent mean ± 1x standard deviation for n = 3 experimental replicates. Axes are logarithmic (base 10) and the dashed grey line represent perfect correlation between nominal concentrations and measured concentrations.

frame as shown in **Fig. S1** (Gardiner et al., 2013; Tian et al., 2024; Vestad et al., 2017).

A Student's T-test was used to compare the different analytical techniques at each concentration measured for the two particles at different nominal concentrations. For 60 nm particles, at the lowest nominal concentration (1.0E11 NP/mL), no significant differences were observed between the singleDLS and htsDLS ($p = 0.057$), but both differed significantly from NTA ($p < 0.05$). At concentrations ≥ 1.0E12 NP/mL, the data of all three instruments were significantly different ($p < 0.05$), suggesting increasing disagreement with rising concentration. For 200 nm particles, only NTA was significantly different at 1.0E9 ($p < 0.05$) while there were no significant differences at 1.0E10 NP/mL. However, at the highest concentration (1.0E11 NP/mL), all comparisons among the instruments showed significant differences ($p < 0.05$).

3.2.3. *Comparing colloidal properties of lipid nanoparticles*

After validating the measurement of colloidal properties for the standard Nanospheres™, LNP were employed as a "real-world" system to compare the singleDLS and htsDLS systems. LNP were loaded with either mRNA or siRNA, and were formulated on a semi-automatic microfluidic system. Flow channels were configured in a T-junction, and the organic:aqueous flow rate ratio (FRR) was maintained at 3:1, while total flow rate (TFR) was varied between 1–3 mL/min (Fig. 5). Other production parameters such as total lipid concentration (5.5 mM), lipid ratios, and N/P ratio were kept constant. This particular combination of lipids and lipid ratios (50 % DLin-MC3-DMA, 38.5 % cholesterol, 10 % DSPC and 1.5 % DMG-PEG_{2k}) was selected as it is comparable to clinically approved Onpattro (siRNA-loaded LNP) (Chen et al., 2016; Ojansivu et al., 2025) and is a conventional formulation widely utilized for LNP (Gambaro et al., 2024; Guo et al., 2024; Kawaguchi et al., 2023; Vigil et al., 2021). This semi-automated approach enabled the investigation of LNP with different colloidal properties based on their production parameters, and allowed verification of the inter-instrument measurement consistency.

LNP colloidal properties were evaluated (d_H and PdI) and then compared with the independent analysis of the correlation function (Fig. 6). For mRNA-loaded LNP, there were no significant difference in d_H between default and independent analysis for either the singleDLS (p-value = 0.526, 0.121, 0.388 when the TFR is 1,2 and 3 mL/min, respectively), or the htsDLS (p-value = 0.148, 0.137 and 0.198 when the TFR is 1,2 and 3 mL/min, respectively). Nor were there differences in d_H for siRNA-loaded LNP between default and independent analysis for either the singleDLS (p-value = 0.787, 0.925 and 0.423 when the TFR is 1,2 and 3 mL/min, respectively), or the htsDLS (p-value = 0.148, 0.374 and 0.407 when the TFR is 1,2 and 3 mL/min, respectively). These data underline that for both instruments the d_H results on samples of LNP remain consistent, even when evaluated with an independent calculation of the d_H distribution. A similar analysis revealed that there were no significant differences in any of the reported PdI values, except for the LNP formulation encapsulating mRNA produced with a TFR of 3 mL/

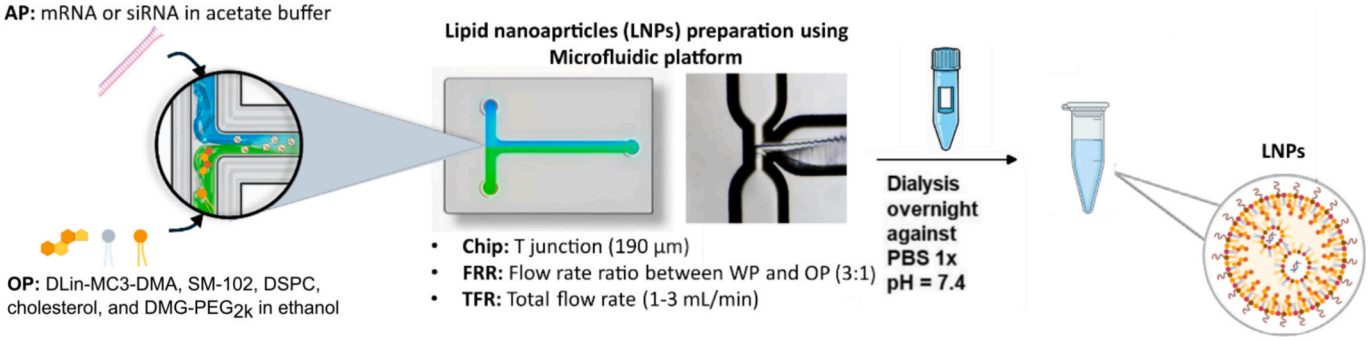

Fig. 5. Schematic diagram of LNPs formulation.

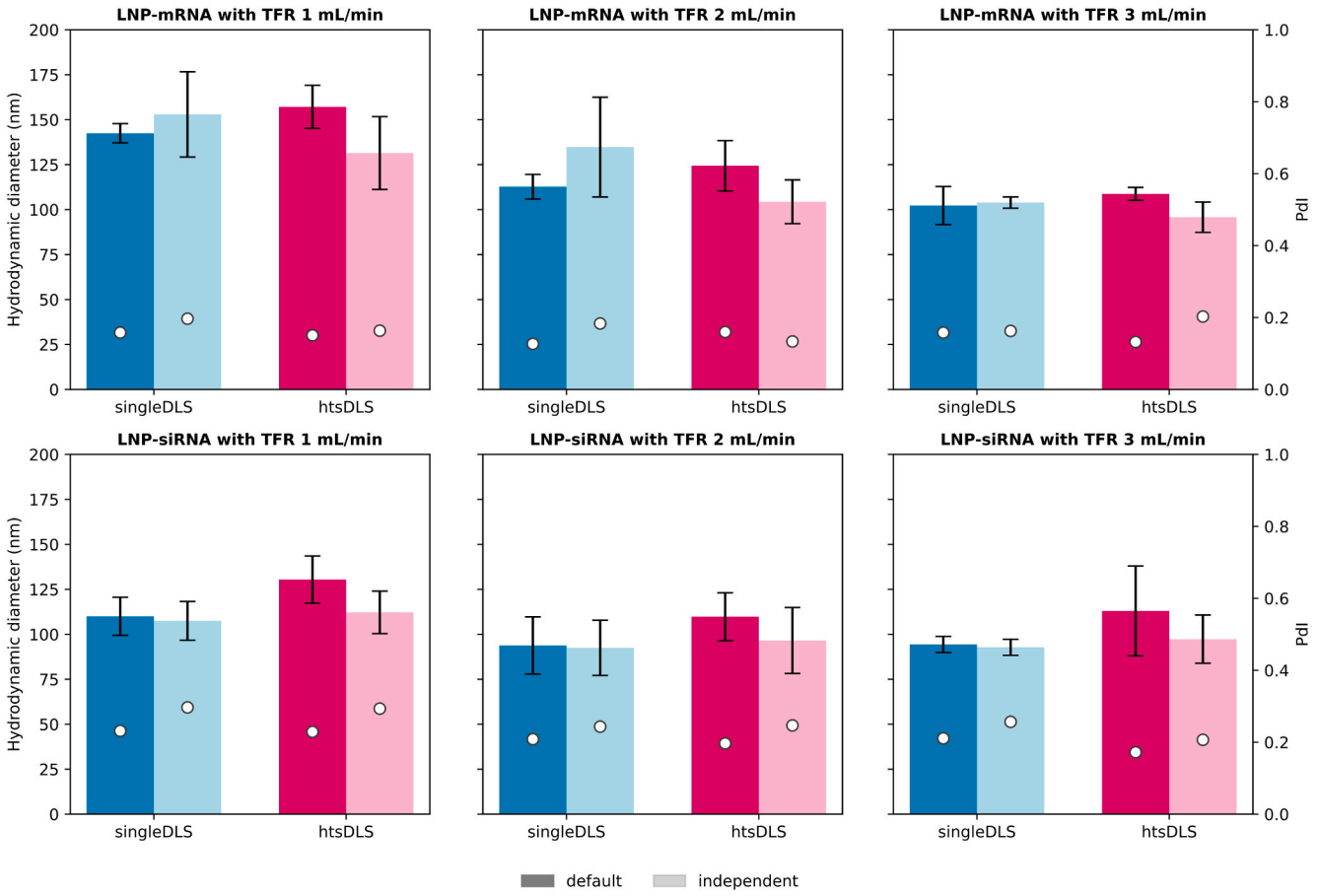

Fig. 6. Comparison between default values for d_H (bars) and polydispersity index (PdI, circles) reported by the instruments, and those calculated independently from the raw auto-correlation function data, using mRNA- and siRNA-loaded LNP produced via microfluidic mixing at three TFRs: 1, 2, and 3 mL/min. Values represent mean ± 1x standard deviation for n = 3 experimental replicates.

min and analyzed by the htsDLS method. This result reinforces the idea that both instruments provide comparable and reliable results.

3.3. RNA loading

The htsDLS combined SLS, DLS and UV/Vis spectroscopy, where payload concentrations can also be reported by demixing the UV/Vis absorbance spectra from the constituent components (e.g. LNP and mRNA). The obvious benefit here is an increased capacity to generate novel formulations and rapidly screen LNP quality attributes. However, we were interested in comparing how such a high-throughput method practically compares to standard assays. To compare the results of the htsDLS with "conventional" characterziation methods (i.e. singleDLS for d_H/dispersity and the RiboGreen assay for RNA loading), LNP were therefore used as a model system.

3.3.1. Validating RNA measurement across instrumentations

First, RNA quantification with the htsDLS platform was compared to the RiboGreen assay. While the RiboGreen assay can similarly be run in a high-throughput format (plate reader assay), the htsDLS offers an all-in-one approach in which DLS and RNA loading are measured almost contemporaneously with no change in sample handling. Thus, the limit of detection (LOD) and limit of quantification (LOQ) were determined for both methods. Standard curves of known concenterations of mRNA or siRNA were measured for each assay in five independent experiments. LOD and LOQ were then calculated as described in Eqs. (3) and (4), respectively, based on best fit linear models (Table 2). It is important to note that R^2 values reported in Fig. 7 represent linear models fit through all 5 standard curve measurements in aggregate, and for each individual experiment the R^2 values ranged from 0.876 to 0.999 (**Table S1**).

Table 2
Limits of detection (LOD) and limits of quantification (LOQ) for the different methods of quantification and payload types (n = 5). The nanomolar (nM) concentrations calculated for mRNA were based on an assumed molecular weight of 320 kDa.

Payload	Method of quantification	LOD	LOQ
mRNA	RiboGreen (w/o Triton X-100)	0.01 µg/mL (0.03 nM)	0.02 µg/mL (0.06 nM)
	RiboGreen (w/ Triton X-100)	0.04 µg/mL (0.13 nM)	0.13 µg/mL (0.41 nM)
	htsDLS	30.69 µg/mL (95.91 nM)	93.01 µg/mL (290.66 nM)
siRNA	RiboGreen (w/o Triton X-100)	0.53 nM	1.60 nM
	RiboGreen (w/ Triton X-100)	0.66 nM	2.01 nM
	htsDLS	501.70 nM	1520.29 nM

The RiboGreen assay and htsDLS measure RNA through two mechanistically different means: the RiboGreen assay through a fluorophore which becomes fluorescent upon binding to nucleotides and the htsDLS based in the UV/Vis absorbance (coupled with spectral unmixing) of RNA and lipids (Cavaluzzi and Borer, 2004; Jones et al., 1998). As a parallel to the htsDLS, mRNA or siRNA content was also measured via UV/Vis absorption at 260 nm on a NanoDrop (**Fig. S2**).

Notably, during experimentation there were significant differences in the limits obtained via the fluorometric assay compared to the UV/

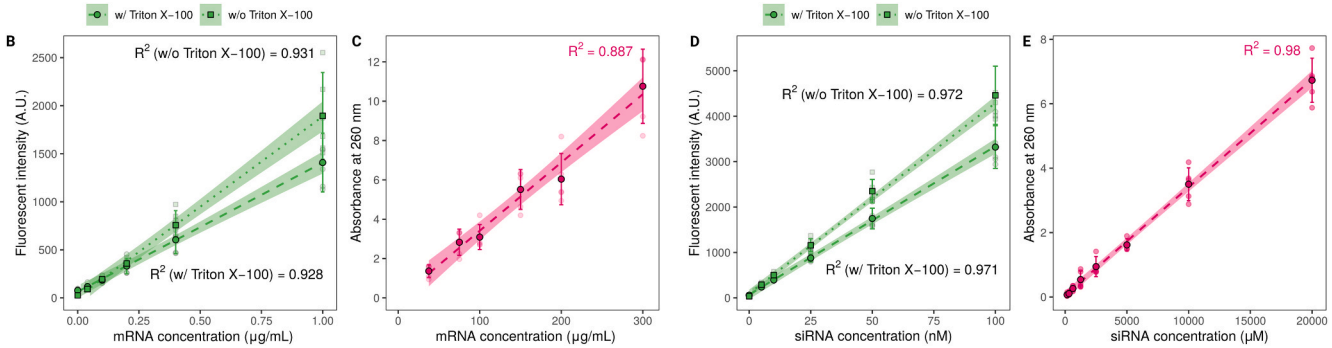

Fig. 7. Standard curves for the quantification of (A,B) mRNA or (C,D) siRNA via the RiboGreen assay or via UV/Vis measurements with the htsDLS. Standard curves represent the average of 5 × independent experimental replicates. Linear models are fit through all experimental points in aggregate.

Vis-based assays. The RiboGreen was significantly more sensitive, reporting LOD approximately 700 × lower than the htsDLS for mRNA and approximately 150 × lower than the htsDLS for siRNA. The differences observed in the LOD between RiboGreen Assay and the htsDLS can be attributed to their different type of detection. Fluorescence-based assays benefit from signal amplification, which improves the signal-to-noise ratio. In contrast, the UV/Vis-based method measures RNA absorbance, which produces a weaker signal and is more sensitive to optical interference from other formulation components (e.g., solvents, lipids), leading to lower sensitivity. Furthermore, RiboGreen shows greater sensitivity for mRNA than for siRNA. This can be explained by the greater molecular size (increased number of nucleotides) of mRNA, which provides more available binding sites for the fluorophore, thus producing a stronger signal. siRNA, being shorter and more structurally compact, has fewer binding sites for RiboGreen which results in a lower signal intensity and reduced sensitivity. Notably, the range of RNA concentrations measured for each type of assay (htsDLS or RiboGreen) had to be adjusted based on the type of RNA (siRNA or mRNA). For example, mRNA was measured between 0.1 to 3.0 nM for the RiboGreen assay versus approximately 100 to 1,000 nM for the htsDLS. Likewise, siRNA was measured between 5 to 100 nM via the RiboGreen assay while the range of siRNA concentrations measured on the htsDLS was approximately 120 to 10,000 nM.

In this context, an analysis of the LOD, as reported in Table 2, reveals that the value of 0.03 nM for mRNA using RiboGreen assay without Triton X-100 reagent, is in good agreement with the results discussed by Jones et al, (1998) who established the sensitivity of the RiboGreen reagent at 1.0 ng/mL (equivalent to approximately 0.02 nM for ribosomal RNA). This agreement underscores the reliability and high sensitivity of the assay. The increase in LOD with Triton X-100 reagent (in particular 0.13 nM for mRNA and 0.66 nM for siRNA) is also consistent with the findings of Bizmark et al, (2024) who demonstrated that detergents could alter the dye-RNA interactions in the RiboGreen assay. Instead, the higher LODs for the htsDLS based on UV/Vis analysis (in particular 93.29 nM for mRNA and 501.70 nM for siRNA) reflect the limitations of absorbance-based measurements, especially for nucleic acids at low concentrations. The higher LOD for siRNA compared to mRNA is attributable to its lower molecular weight, requiring higher molar concentrations to measure absorbance. These values are in perfect agreement with the study of Gallagher (2011), who underscore that UV/Vis spectroscopy at 260 nm has a range generally from 1 to 50 µg/mL for nucleic acids (corresponding to approximately 100 nM to 5 µM for DNA, depending on size). Furthermore, this method is also highly sensitive to optical interference caused by lipid nanoparticles and their components, which can lead to overestimation of RNA concentration or reduced accuracy.

3.3.2. *Characterization of RNA payload encapsulation in LNP*

LNP loading was measured after defining the LOD and LOQ for each instrument and validating the measurement of both mRNA and siRNA. After formulating the LNP with either RNA payload at different TFR, the quantity of total mRNA (Fig. 8A) or siRNA (Fig. 8C) were measured via either the RiboGreen assay or the htsDLS. For mRNA, we observed that the htsDLS tended to report values lower than the RiboGreen assay. One rationale for this is that the theoretical amount of mRNA in this formulation, based on the amount of mRNA in the initial aqueous phase and the volumes recovered after dialysis, is below the LOD for the htsDLS. However, there was only one mRNA-LNP formulation where there was a statistically significant difference between % mRNA entrapment yield measured via RiboGreen and htsDLS (TFR 1 mL/min, p-value = 0.05). For all others there was no statistically significant difference. What is evident is that the htsDLS is more effective than a purely UV/Vis-based approach (i.e. NanoDrop), and reports trends comparable to the RiboGreen assay. When comparing % siRNA entrapment yield between the htsDLS and RiboGreen assay, only the formulation produced at TFR 2 mL/min showed a statistically significant difference (p-value = 0.04).

An additional limitation for UV/Vis-based measurements (the htsDLS and NanoDrop), is that unlike the RiboGreen assay, UV/Vis-

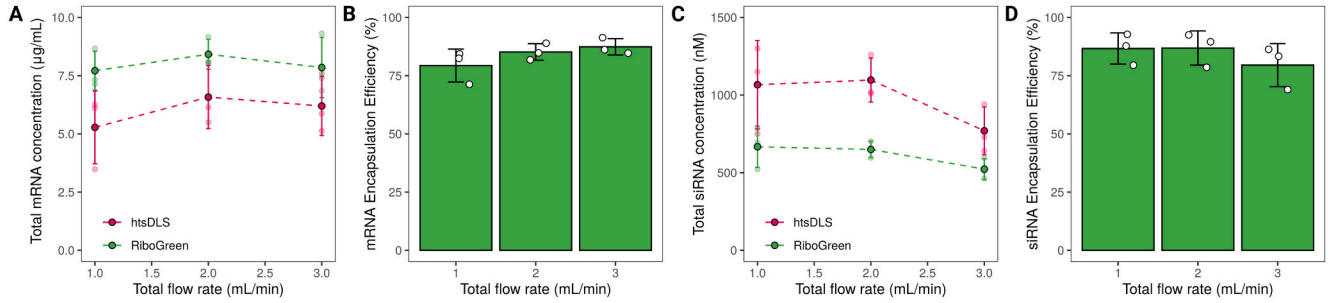

Fig. 8. Loading of RNA in LNP. Total amount of (A) mRNA or (C) siRNA measured by either the Ribo Green assay or via the htsDLS instrument for LNP prepared at different total flow rates. Encapsulation efficiency (% internal vs total RNA) of the LNP loaded with (B) mRNA or (D) siRNA as a function of TFR (1, 2 and 3 mL/min) as evaluated by the RiboGreen assay. Data shows the mean ± standard deviation for n = 3 experimental replicates.

based measurements are unable to distinguish between unencapsulated and encapsulated RNA. Because the RiboGreen assay is able to distinguish between unencapsulated and encapsulated RNA, we report the encapsulation efficiency (i.e. percent of internal encapsulated RNA over total RNA measured, Fig. 8B, D). The results revealed between 80 % and 90 % of RNA is captured internally for all LNP. mRNA-loaded LNP showed a progressive increase of encapsulation efficiency at higher TFR (Fig. 8B), while siRNA-loaded LNP showed the opposite trend (Fig. 8D). These results suggest that for each formulation the encapsulation efficiency, as well as the % entrapment yield of payload recovered (**Fig. S3**), depends on the TFR and type of cargo/cargo molecular weight.

These data have shown how the htsDLS compares to conventional singleDLS and RiboGreen assays for measuring size/PdI and RNA loading, respectively. To evaluate how general this process could be across LNP formulations, we formulated LNPs with a different ionizable lipid (SM-102) and at a different N/P ratio (10:1). This formulation was produced on the microfluidic system at a TFR of 3 mL/min and an aqueous:organic FRR of 3:1. **Fig. S4A** shows the hydrodynamic diameter and PdI of the SM-102 LNP, and singleDLS and htsDLS showed very similar results. Likewise, measurements of total mRNA loading showed a similar trend where the RiboGreen assay measured more total RNA in comparison with the htsDLS.

4. Conclusion

The emergence of automation in nanoparticle production and characterization has the potential to rapidly increase the throughput in which hit nanomedicine formulations can be identified through high-throughput screening. However, it is critical that the quality attributes of nanomedicines developed via high-throughput screening remain consistent as that formulation is developed from screening approach through production scale, and there must be parity between high-throughput screening methods and conventionally accepted methods of nano-characterization. Here, an in-depth analysis comparing "gold standard" approachs in lipid nanoparticle characterization are validated in a high-throughput workflow. Demonstrating that data obtained from high-throughput platforms are consistent is a fundamental requirement to ensure the robustness of the pharmaceutical development process, data reproducibility, and transferability of the best formulations-fundamental aspects for translational medicine and industry.

We report here a technical analysis comparing conventional techniques for characterizing LNP attributes (d_H, dispersity, and RNA loading) with a high-throughput plate-reader based approach. We observed that, for the measurement of colloidal properties, the htsDLS provides results comparable to conventional one-at-a-time DLS (or NTA). However, for RNA quantification, in particular at low concentrations, the sensitivity of the plate reader, UV/Vis-based approach appears lower compared to the RiboGreen assay. This is especially apparent for mRNA. Thus, as a tool the plate-reader UV/Vis approach is useful for rapid screening, but additional confirmation of RNA payload loading via other (e.g. fluorescence-based) assays is necessary for accuracy. These results show how the integration of microfluidic production with automated characterization is an important step for the efficient and scalable development of LNP, with important applications in clinical and pharmaceutical fields.

CRediT authorship contribution statement

Simone Misto: Writing – original draft, Writing – review & editing, Visualization, Investigation, Formal analysis. **Teresa Ferrillo:** Writing – original draft, Methodology. **Sandor Balog:** Writing – original draft, Software, Methodology, Formal analysis. **Fabiana Quaglia:** Writing – original draft, Writing – review & editing, Resources, Project administration, Funding acquisition. **Thomas Lee Moore:** Writing – original draft, Writing – review & editing, Visualization, Supervision, Methodology, Formal analysis, Conceptualization.

Declaration of competing interest

The authors declare that they have no known competing financial interests or personal relationships that could have appeared to influence the work reported in this paper.

Acknowledgements

This work was supported by the grant CN00000041 "National Center for Gene Therapy and Drugs based on RNA Technology" (concession number 1035 on June 17, 2022 under PNRR MUR-M4C2-Investment 1.4 Call "National Centers," financed by the EU-NextGenerationEU), project code E63C22000940007.

Appendix A. Supplementary material

Supplementary data to this article can be found online at https://doi.org/10.1016/j.ijpharm.2026.126581.

Data availability

Data will be made available on request.

References

Austin, J., Minelli, C., Hamilton, D., Wywijas, M., Jones, H.J., 2020. Nanoparticle number concentration measurements by multi-angle dynamic light scattering. J. Nanoparticle Res. 22, 108. https://doi.org/10.1007/s11051-020-04840-8.

Bizmark, N., Nayagam, S., Kim, B., Amelemah, D.F., Zhang, D., Datta, S.S., Priestley, R. D., Colace, T., Wang, J., Prud'homme, R.K., 2024. Ribogreen Fluorescent Assay Kinetics to Measure Ribonucleic Acid Loading into Lipid Nanoparticle Carriers. Adv. Mater. Interfaces 11, 2301083. Doi: 10.1002/admi.202301083.

Cavaluzzi, M.J., Borer, P.N., 2004. Revised UV extinction coefficients for nucleoside-5′-monophosphates and unpaired DNA and RNA. Nucleic Acids Res. 32, e13–e. https://doi.org/10.1093/nar/gnh015.

Chen, S., Tam, Y.Y.C., Lin, P.J.C., Sung, M.M.H., Tam, Y.K., Cullis, P.R., 2016. Influence of particle size on the in vivo potency of lipid nanoparticle formulations of siRNA. J. Control. Release 235, 236–244. https://doi.org/10.1016/j.jconrel.2016.05.059.

Coley, C.W., Thomas, D.A., Lummiss, J.A.M., Jaworski, J.N., Breen, C.P., Schultz, V., Hart, T., Fishman, J.S., Rogers, L., Gao, H., Hicklin, R.W., Plehiers, P.P., Byington, J., Piotti, J.S., Green, W.H., Hart, A.J., Jamison, T.F., Jensen, K.F., 2019. A robotic platform for flow synthesis of organic compounds informed by AI planning. Science 365, eaax1566. https://doi.org/10.1126/science.aax1566.

Cui, L., Hunter, M.R., Sonzini, S., Pereira, S., Romanelli, S.M., Liu, K., Li, W., Liang, L., Yang, B., Mahmoudi, N., Desai, A.S., 2022. Mechanistic studies of an automated lipid nanoparticle reveal critical pharmaceutical properties associated with enhanced mRNA functional delivery in vitro and in vivo. Small 18, 2105832. https://doi.org/10.1002/smll.202105832.

Cui, L., Pereira, S., Sonzini, S., Van Pelt, S., Romanelli, S.M., Liang, L., Ulkoski, D., Krishnamurthy, V.R., Brannigan, E., Brankin, C., Desai, A.S., 2022. Development of a high-throughput platform for screening lipid nanoparticles for mRNA delivery. Nanoscale 14, 1480–1491. https://doi.org/10.1039/D1NR06858J.

Cullis, P.R., Felgner, P.L., 2024. The 60-year evolution of lipid nanoparticles for nucleic acid delivery. Nat. Rev. Drug Discov. 23, 709–722. https://doi.org/10.1038/s41573-024-00977-6.

Dauer, K., Pfeiffer-Marek, S., Kamm, W., Wagner, K.G., 2021. Microwell plate-based dynamic light scattering as a high-throughput characterization tool in biopharmaceutical development. Pharmaceutics 13, 172. https://doi.org/10.3390/pharmaceutics13020172.

Dolgin, E., 2021. The tangled history of mRNA vaccines. Nature 597, 318–324. https://doi.org/10.1038/d41586-021-02483-w.

Fan, Y., Yen, C.-W., Lin, H.-C., Hou, W., Estevez, A., Sarode, A., Goyon, A., Bian, J., Lin, J., Koenig, S.G., Leung, D., Nagapudi, K., Zhang, K., 2021. Automated high-throughput preparation and characterization of oligonucleotide-loaded lipid nanoparticles. Int. J. Pharm. 599, 120392. https://doi.org/10.1016/j.ijpharm.2021.120392.

Frisken, B.J., 2001. Revisiting the method of cumulants for the analysis of dynamic light-scattering data. Appl. Opt. 40, 4087. https://doi.org/10.1364/AO.40.004087.

Gallagher, S.R., 2011. Quantitation of DNA and RNA with Absorption and Fluorescence Spectroscopy. Curr. Protoc. Mol. Biol. 93, A.3D.1-A.3D.14. Doi: 10.1002/0471142727.mba03ds93.

Gambaro, R., Rivero Berti, I., Limeres, M.J., Huck-Iriart, C., Svensson, M., Fraude, S., Pretsch, L., Si, S., Lieberwirth, I., Gehring, S., Cacicedo, M., Islan, G.A., 2024. Optimizing mRNA-loaded lipid nanoparticles as a potential tool for protein-replacement therapy. Pharmaceutics 16, 771. https://doi.org/10.3390/pharmaceutics16060771.

Gardiner, C., Ferreira, Y.J., Dragovic, R.A., Redman, C.W.G., Sargent, I.L., 2013. Extracellular vesicle sizing and enumeration by nanoparticle tracking analysis. J. Extracell. Vesicles 2, 19671. https://doi.org/10.3402/jev.v2i0.19671.

Guo, Z., Zeng, C., Shen, Y., Hu, L., Zhang, H., Li, Z., Dong, W., Wang, Q., Liu, Q., Wang, Y., Jiang, W., 2024. Helper lipid-enhanced mRNA delivery for treating metabolic dysfunction-associated fatty liver disease. Nano Lett. 24, 6743–6752. https://doi.org/10.1021/acs.nanolett.4c01458.

Hickman, R.J., Bannigan, P., Bao, Z., Aspuru-Guzik, A., Allen, C., 2023. Self-driving laboratories: a paradigm shift in nanomedicine development. Matter 6, 1071–1081. https://doi.org/10.1016/j.matt.2023.02.007.

Jones, L.J., Yue, S.T., Cheung, C.-Y., Singer, V.L., 1998. RNA quantitation by fluorescence-based solution assay: ribogreen reagent characterization. Anal. Biochem. 265, 368–374. https://doi.org/10.1006/abio.1998.2914.

Kawaguchi, M., Noda, M., Ono, A., Kamiya, M., Matsumoto, M., Tsurumaru, M., Mizukami, S., Mukai, H., Kawakami, S., 2023. effect of cholesterol content of lipid composition in mRNA-LNPs on the protein expression in the injected site and liver after local administration in mice. J. Pharm. Sci. 112, 1401–1410. https://doi.org/10.1016/j.xphs.2022.12.026.

Koppel, D.E., 1972. Analysis of macromolecular polydispersity in intensity correlation spectroscopy: the method of cumulants. J. Chem. Phys. 57, 4814–4820. https://doi.org/10.1063/1.1678153.

Le Ru, E.C., Böttger, R., Andrews, D., Baumhof, P., Rakonjac, J.V., Laufersky, G., Darby, B.L., 2025. Rapid and accurate quantification of RNA in lipid nanoparticles by scatter-free UV/visible spectroscopy. Nano Lett. 25, 6813–6819. https://doi.org/10.1021/acs.nanolett.5c01491.

Liu, L., Bi, M., Wang, Y., Liu, J., Jiang, X., Xu, Z., Zhang, X., 2021. Artificial intelligence-powered microfluidics for nanomedicine and materials synthesis. Nanoscale 13, 19352–19366. https://doi.org/10.1039/d1nr06195j.

Liu, X., Dai, Q., Austin, L., Coutts, J., Knowles, G., Zhou, J., Chen, H., Huo, Q., 2008. A one-step homogeneous immunoassay for cancer biomarker detection using gold nanoparticle probes coupled with dynamic light scattering. J. Am. Chem. Soc. 130, 2780–2782. https://doi.org/10.1021/ja711298.

Maguire, C.M., Rösslein, M., Wick, P., Prina-Mello, A., 2018. Characterisation of particles in solution – a perspective on light scattering and comparative technologies. Sci. Technol. Adv. Mater. 19, 732–745. https://doi.org/10.1080/14686996.2018.1517587.

Mailer, A.G., Clegg, P.S., Pusey, P.N., 2015. Particle sizing by dynamic light scattering: non-linear cumulant analysis. J. Phys. Condens. Matter 27, 145102. https://doi.org/10.1088/0953-8984/27/14/145102.

Mohr, J., Chuan, Y.P., Wu, Y., Lua, L.H.L., Middelberg, A.P.J., 2013. Virus-like particle formulation optimization by miniaturized high-throughput screening. Methods 60, 248–256. https://doi.org/10.1016/j.ymeth.2013.04.019.

Ojansivu, M., Barriga, H.M.G., Holme, M.N., Morf, S., Doutch, J.J., Andaloussi, S.E., Kjellman, T., Johnsson, M., Barauskas, J., Stevens, M.M., 2025. Formulation and characterization of novel ionizable and cationic lipid nanoparticles for the delivery of splice-switching oligonucleotides. Adv. Mater. 37. https://doi.org/10.1002/adma.202419538.

Shang, J., Gao, X., 2014. Nanoparticle counting: towards accurate determination of the molar concentration. Chem. Soc. Rev. 43, 7267–7278. https://doi.org/10.1039/C4CS00128A.

Shepherd, S.J., Han, X., Mukalel, A.J., El-Mayta, R., Thatte, A.S., Wu, J., Padilla, M.S., Alameh, M.-G., Srikumar, N., Lee, D., Weissman, D., Issadore, D., Mitchell, M.J., 2023. Throughput-scalable manufacturing of SARS-CoV-2 mRNA lipid nanoparticle vaccines. Proc. Natl. Acad. Sci. 120, e2303567120. https://doi.org/10.1073/pnas.2303567120.

Stetefeld, J., McKenna, S.A., Patel, T.R., 2016. Dynamic light scattering: a practical guide and applications in biomedical sciences. Biophys. Rev. 8, 409–427. https://doi.org/10.1007/s12551-016-0218-6.

Tian, Y., Tian, D., Peng, X., Qiu, H., 2024. Critical parameters to standardize the size and concentration determination of nanomaterials by nanoparticle tracking analysis. Int. J. Pharm. 656, 124097. https://doi.org/10.1016/j.ijpharm.2024.124097.

Vestad, B., Llorente, A., Neurauter, A., Phuyal, S., Kierulf, B., Kierulf, P., Skotland, T., Sandvig, K., Haug, K.B.F., Øvstebø, R., 2017. Size and concentration analyses of extracellular vesicles by nanoparticle tracking analysis: a variation study. J. Extracell. Vesicles 6, 1344087. https://doi.org/10.1080/20013078.2017.1344087.

Vigil, T.N., Zhang-Hulsey, D., Santos, J.L., Patrick Hussmann, G., 2021. Expediting in vitro characterization of mRNA-based gene therapies via high-content fluorescent imaging. Anal. Biochem. 627, 114259. https://doi.org/10.1016/j.ab.2021.114259.

Vysotskii, V.V., Uryupina, O.Y., Gusel'nikova, A.V., Roldugin, V.I., 2009. On the feasibility of determining nanoparticle concentration by the dynamic light scattering method. Colloid J 71, 739–744. https://doi.org/10.1134/S1061933X09060027.

Yoo, S., Han, E.L., Murray, A.M., Kim, D., Bang, E.-K., Mitchell, M.J., 2025. High-throughput formulation using fast mRNA lipid nanoparticle assembly via simple thermomixing (HTF-FLASH). Nano Lett. 25, 14695–14703. https://doi.org/10.1021/acs.nanolett.5c03793.